Guidance-based Path Following Control of the Powered Parafoil

Erlin Zhu*, Haitao Gao**

** School of Electrical & Information Engineering, Jiangsu University of Technology, Changzhou, 213001, China (e-mail: elzhu@jsut.edu.cn).*
*** College of Electrical and Electronic Engineering, Anhui Science and Technology University, Fengyang, 233100, China (e-mail:gc_0532@126.com)*

Abstract: The powered parafoil is a new kind of flexible vehicle, which consists of the parafoil system and engine propeller system. Compared with common parafoil systems, the powered parafoil has better maneuverability. Aiming at eight degrees of freedom (DOF) nonlinear dynamic model, a path following control method for the vehicle is presented. The position error from the desired path is transformed to guidance laws of azimuth angle and inclination angle. In the process of control system design, internal coupling of the model and external gust disturbance are observed by extended state observer (ESO) of linear active disturbance rejection control (LADRC) and eliminated in control law. The simulation results verify the effectiveness and robustness of the method.

Keywords: Powered parafoil, Path following control, Guidance law, Linear active disturbance rejection control (LADRC)

1. INTRODUCTION

As a new aircraft with flexible wing, the powered parafoil consists of the common parafoil system and engine propeller system which equipped on the payload. Powered parafoil has better maneuverability than traditional parafoil systems (Chambers, 2007). Besides the turning motion when one side steering line is pulled down, and flare-landing when the both sides of steering lines are pulled down to the maximum quickly and simultaneously, hovering and even climbing can be achieved through controlling the thrust provided by engine propeller system(Li et al., 2015; Ghoreyshi et al., 2016). By right of the special aerodynamic characteristics, the application of the powered parafoil has been expanded to wilder fields, such as airdrop of materials, environmental monitoring, agricultural seeding, advertisement propaganda, and so on. The flight control is the key of safe flight and task execution for the powered parafoil.

The current research (Goodrick, 1981; Barrows, 2002; Slegers et al., 2009; Tao et al., 2016; Zhang et al., 2018) mainly focus on six degrees of freedom (DOF) parafoil systems, which consider the canopy and payload as a rigid body. Aiming at relative motion between the canopy and payload, (Muller et al., 2003; Xiong, 2005; Slegers, 2010) studied eight DOF nonlinear dynamic model of parafoils. (Aoustin et al., 2012) simplified the model of the powered parafoil, and studied its vertical motion. Based on a simple static model, (Yang et al., 2013) studied longitudinal flight performances of the powered parafoil. (Watanabe et al., 2008) considered the effect of friction of the connection point between the canopy and payload in force analysis, and built the eight DOF nonlinear dynamic model of the powered paraglider (PPG). (Zhu et al., 2015) studied the eight DOF dynamic model of the powered parafoil based on Kirchhoff motion equation, and analyzed the aerodynamic characteristics.

The above-mentioned research focus on the modeling of the powered parafoil. From the published literatures, there are few works about the control on powered parafoils. (Ochi et al., 2009) derived the linear dynamic model of the powered parafoil according to the nonlinear model, and designed the PID controller. According to vertical model of the powered parafoil, (Aoustin et al., 2012) used the method of part feedback linearization for designing nonlinear control algorithm on vertical trajectory control. (Chen et al., 2016) used backstepping method for altitude control of unmanned powered parafoil. (Chen et al., 2017) also did research on longitudinal control of unmanned powered parafoil. But they did not consider horizontal motion control of the powered parafoil, and the controller relied on the exact mathematical model. (Tan et al., 2017) studied the trajectory tracking of powered parafoil based on characteristic model based all-coefficient adaptive control, but concrete guidance methods were not given.

Compared with trajectory tracking control, smoother convergence to the path is achieved when path following strategies are used (Xiang et al., 2009; Zheng et al., 2013b). In this paper, the issue of the guidance-based control for the powered parafoil is studied. The desired path is parameterized in path following strategy. As for motion control of eight DOF powered parafoil, guidance laws of lateral and vertical motions are obtained through Lyapunov method. Linear active disturbance rejection control (LADRC) controllers in lateral and vertical channels are designed.

The innovation work is to introduce the guidance theory to the powered parafoil path following control to enhance the stability of the system. For uncertainties of the model, external disturbances and internal coupling of two channels, design extended state observer (ESO) to observe the total disturbance which can be compensated in control law.

The rest of this paper is arranged as follows. In section 2, the overview of modelling for the powered parafoil is given. In section 3, the path following strategy based on guidance for the powered parafoil is proposed. In section 4, aiming at dynamic characteristics of the powered parafoil and the path following strategy, LADRC controllers are designed in lateral and vertical channels. In section5, numerical simulations are carried out to verify the path following control algorithm. The last section includes the summary and expectation of the studies in this paper.

2. DYNAMIC MODEL OF THE POWERD PARAFOIL

The eight DOF dynamic model of the powered parafoil which has been built by the author (Zhu et al., 2015) is chosen as the controlled object in this paper. On the basis of six DOF, the other two DOF (the relative yaw motion and the relative pitch motion of two bodies) are considered. In this section, only the main formulas are given, and more details about the model and dynamic characteristics are referred to the reference.

To facilitate the establishment of the model, some reasonable hypotheses are made as follows.

(1) When the canopy is fully inflated, the aerodynamic configuration remains unchanged without maneuvering;

(2) The mass center of canopy coincides with the aerodynamic pressure center, but does not coincide with the gravity center;

(3) Ignoring the lift of the payload, only the aerodynamic drag is considered;

(4) The ground is a plane.

2.1 Dynamic equation of the payload

The payload is considered to be a regular-shaped rigid body, such that the theorems of momentum and moment of momentum are used for motion equations of the payload. External force mainly consists of aerodynamic force, gravity, thrust provided by engine propeller system and the tension of suspension line. Assuming that gravity and thrust both act on the mass center of the payload, the moments formed by gravity and thrust can be neglected in the motion equations, shown as (1), (2).

$$\frac{\partial \boldsymbol{P}_w}{\partial t} + \boldsymbol{W}_w \times \boldsymbol{P}_w = \boldsymbol{F}_w^{aero} + \boldsymbol{F}_w^{G} + \boldsymbol{F}_w^{t} + \boldsymbol{F}_w^{th} \tag{1}$$

$$\frac{\partial \boldsymbol{H}_w}{\partial t} + \boldsymbol{W}_w \times \boldsymbol{H}_w = \boldsymbol{M}_w^{aero} + \boldsymbol{M}_w^{fr} + \boldsymbol{M}_w^{t} \tag{2}$$

$\boldsymbol{P}, \boldsymbol{H}$ are momentum and moment of momentum. $\boldsymbol{W} = \begin{bmatrix} p & q & r \end{bmatrix}^{\mathrm{T}}$ denotes the angle velocity vector, and p, q, r denote rotational angular velocity around three axes respectively. $\boldsymbol{F}, \boldsymbol{M}$ are the force and moment. Subscript w represents the payload frame. Superscript $aero$ represents the aerodynamic force, G represents gravity, fr represents friction, th represents thrust, and t represents tension. $\times$ denotes the cross product.

2.2 Dynamic equation of the parafoil

The canopy is made of flexible fabric, such that the motion of the apparent mass should be taken into account. The motion equation of rigid body might lead to errors, and is not applicable to the parafoil.

After the canopy is inflated, the force acting on the parafoil mainly consists of aerodynamic force, gravity, and the tension of lines. The Kirchhoff motion equation is used for dynamic equation of the parafoil which is expressed as (3), (4).

$$\frac{\partial \boldsymbol{P}_s}{\partial t} + \boldsymbol{W}_s \times \boldsymbol{P}_s = \boldsymbol{F}_s^{aero} + \boldsymbol{F}_s^{G} + \boldsymbol{F}_s^{t} \tag{3}$$

$$\frac{\partial \boldsymbol{H}_s}{\partial t} + \boldsymbol{W}_s \times \boldsymbol{H}_s + \boldsymbol{V}_s \times \boldsymbol{P}_s = \boldsymbol{M}_s^{aero} + \boldsymbol{M}_s^{G} + \boldsymbol{M}_s^{fr} + \boldsymbol{M}_s^{t} \tag{4}$$

$\boldsymbol{V} = \begin{bmatrix} u & v & w \end{bmatrix}^{\mathrm{T}}$ denotes the velocity vector, and u, v, w denote translational velocity along three axes respectively. The subscript s represents the parafoil frame. Definitions of other variables are the same as (1), (2).he

2.3 Handling of constraints

The relative rotation between the payload and parafoil is expressed as follows.

$$\boldsymbol{W}_w = \boldsymbol{W}_s + \boldsymbol{\tau}_s + \boldsymbol{\kappa}_w \tag{5}$$

Where $\boldsymbol{\tau}_s = \begin{bmatrix} 0 & 0 & \dot{\psi}_r \end{bmatrix}^{\mathrm{T}}$ with respect to the parafoil frame. ψ_r represents the relative yaw angle. $\boldsymbol{\kappa}_w = \begin{bmatrix} 0 & \dot{\theta}_r & 0 \end{bmatrix}^{\mathrm{T}}$ with respect to the payload frame. θ_r represents the relative pitch angle.

Taking derivative of (5), constraint relationship of angular accelerations is obtained.

$$\boldsymbol{T}_{w-s}\dot{\boldsymbol{W}}_w - \dot{\boldsymbol{W}}_s - \boldsymbol{T}_{w-s}\dot{\boldsymbol{\kappa}}_w - \dot{\boldsymbol{\tau}}_s = \left(\boldsymbol{W}_s - \boldsymbol{T}_{w-s}\boldsymbol{W}_w\right) \times \boldsymbol{W}_s - (\boldsymbol{T}_{w-s}\boldsymbol{\kappa}_w) \times \boldsymbol{\tau}_s \tag{6}$$

$\boldsymbol{T}_{w-s}$ is the transformation matrix from the payload frame to the parafoil frame.

Choose $\boldsymbol{x} = \begin{bmatrix} \boldsymbol{V}_w^{\mathrm{T}} & \boldsymbol{W}_w^{\mathrm{T}} & \boldsymbol{V}_s^{\mathrm{T}} & \boldsymbol{W}_s^{\mathrm{T}} & \dot{\psi}_r & \dot{\theta}_r \end{bmatrix}^{\mathrm{T}}$ as the state vector of the system. Based on (1)-(4) and (6), the dynamic model is as follows:

$$\dot{\boldsymbol{x}} = (\begin{bmatrix} \boldsymbol{D}_1^{\mathrm{T}} & \boldsymbol{D}_2^{\mathrm{T}} & \boldsymbol{D}_3^{\mathrm{T}} & \boldsymbol{D}_4^{\mathrm{T}} \end{bmatrix}^{\mathrm{T}})^{-1} \begin{bmatrix} \boldsymbol{E}_1^{\mathrm{T}} & \boldsymbol{E}_2^{\mathrm{T}} & \boldsymbol{E}_3^{\mathrm{T}} & \boldsymbol{E}_4^{\mathrm{T}} \end{bmatrix}^{\mathrm{T}} \tag{7}$$

$\boldsymbol{D}_i$ and $\boldsymbol{E}_i$ $\left(i = 1, \cdots, 4\right)$ are the matrixes about parameters and state variables of the powered parafoil.

3. GUIDANCE-BASED PATH FOLLOWING STRATEGY

With the development of GPS and aerospace technology, the acquirements on the vehicles are getting higher and higher. The guidance theory is applied to the field of vehicle control

(Zheng et al., 2013a; Zheng et al., 2013b; Zheng et al., 2014). In this paper, inspired by the theory of guidance-based path following (Breivik et al., 2005; Breivik et al., 2008), the guidance-based path following strategy for the powered parafoil is proposed.

The following hypotheses are made.

(1) The desired path is regular shape path, and can be regularly parameterized;

(2) The velocity of the desired point on the desired path is lower-bounded and non-negative.

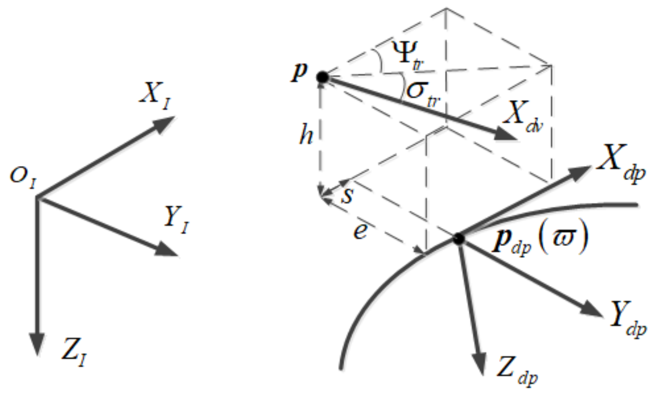

Fig. 1. The schematic diagram of the three-dimension path following.

The frame $O_I X_I Y_I Z_I$ denotes earth reference frame (ERF). Point $\boldsymbol{p}$ denotes the mass position of the powered parafoil in 3D space, whose position and velocity are denoted as $\boldsymbol{p} = [x\ y\ z]^{\mathrm{T}}$ and $\dot{\boldsymbol{p}} = [\dot{x}\ \dot{y}\ \dot{z}]^{\mathrm{T}}$, respectively. The direction of the velocity can be described through azimuth angle Ψ and inclination angle σ. The definition of Ψ is the angle between velocity direction and positive direction of X_I, shown as:

$$\Psi = \arctan\left(\frac{\dot{y}}{\dot{x}}\right).$$

The definition of σ is the angle between velocity direction and horizontal plane, shown as:

$$\sigma = \arctan\left(\frac{-\dot{z}}{\sqrt{\dot{x}^2 + \dot{y}^2}}\right).$$

σ is positive when the path is ascending, and the angle is negative when the path is descending.

$\boldsymbol{p}_{dp}(\varpi)$ denotes the point on the desired path, and is always moving along the desired path, which is updated through scaling variable ϖ. Aiming at the desired path, the path reference frame (PRF) is built. The desired point $\boldsymbol{p}_{dp}(\varpi)$ is chosen as the origin of frame. X_{dp} is along the velocity direction of the desired point, and Z_{dp} is perpendicular to X_{dp}. The plane that constituted by the two axes is perpendicular to the horizontal plane. Rotating Ψ_{dp} around Z_I, transition reference frame (TRF) is obtained. Transform relation is represented as the following matrix.

$$\boldsymbol{T}_{Z_I}(\Psi_{dp}) = \begin{bmatrix} \cos\Psi_{dp} & \sin\Psi_{dp} & 0 \\ -\sin\Psi_{dp} & \cos\Psi_{dp} & 0 \\ 0 & 0 & 1 \end{bmatrix} \tag{8}$$

Then rotating σ_{dp} around the axis Y of TRF, the PRF is obtained. The transform matrix is as follows.

$$\boldsymbol{T}_{Y_I}(\sigma_{dp}) = \begin{bmatrix} \cos\sigma_{dp} & 0 & -\sin\sigma_{dp} \\ 0 & 1 & 0 \\ \sin\sigma_{dp} & 0 & \cos\sigma_{dp} \end{bmatrix} \tag{9}$$

The transformation matrix from ERF to PRF can be expressed as follows.

$$\boldsymbol{T}_{I-p} = \boldsymbol{T}_{Y_I}(\sigma_{dp})\boldsymbol{T}_{Z_I}(\Psi_{dp}) \tag{10}$$

The position error between the point and the desired point in the space is transformed to PRF.

$$\boldsymbol{\varepsilon} = \boldsymbol{T}_{I-p}\left(\boldsymbol{p} - \boldsymbol{p}_{dp}(\varpi)\right) \tag{11}$$

$\boldsymbol{\varepsilon} = [s\ e\ h]^T$, s denotes forward error, e denotes lateral error, and h denotes vertical error, shown as Fig. 1.

To facilitate the following derivation, the velocity reference frame (VRF) is built. The following velocity transform relation can be obtained.

$$\dot{\boldsymbol{p}} = \boldsymbol{T}_{v-I}\boldsymbol{V}_{ve} \tag{12}$$

where $\boldsymbol{V}_{ve} = [U_{ve}\quad 0\quad 0]^T$ denotes the velocity in VRF, and $\boldsymbol{T}_{v-I}$ denotes transformation matrix from VRF to ERF.

$$\boldsymbol{T}_{v-I} = \boldsymbol{T}_{I-p}^{\mathrm{T}}\boldsymbol{T}_{v-p} \tag{13}$$

where $\boldsymbol{T}_{v-p} = \boldsymbol{T}_{Z_v}^{\mathrm{T}}(\Psi_{tr})\boldsymbol{T}_{Y_v}^{\mathrm{T}}(\sigma_{tr})$.

Similar to (12), the derivative of $\boldsymbol{p}_{dp}$ can be expressed as

$$\dot{\boldsymbol{p}}_{dp} = \boldsymbol{T}_{I-p}^{\mathrm{T}}\boldsymbol{V}_{dp}. \tag{14}$$

where $\boldsymbol{V}_{dp} = [U_{dp}\quad 0\quad 0]^{\mathrm{T}}$ is the velocity of the desired point in PRF.

The desired path is updated through the scaling variable ϖ. According to (14), the rate of change of ϖ is obtained as follows.

$$\dot{\varpi} = \frac{U_{dp}}{\sqrt{x_{dp}'^{\,2} + y_{dp}'^{\,2} + z_{dp}'^{\,2}}} \tag{15}$$

The research in this paper focus on the phase of task execution of the powered parafoil, where the attitude of the desired path is unchanged, and the horizontal path is the standard circular path. The attitude of the desired path is unchanged, and the desired point is just moving in horizontal plane along the desired path. The Z axes of ERF and PRF are parallel, such that the transformation angle σ_{tr} is equal to inclination angle σ_{pp} of the powered parafoil, and $\sigma_{dp} = 0$. According to (13),

$$\boldsymbol{T}_{v-p} = \boldsymbol{T}_{I-p}\boldsymbol{T}_{v-I}$$
$$= \begin{bmatrix} \cos\Psi_{dp} & \sin\Psi_{dp} & 0 \\ -\sin\Psi_{dp} & \cos\Psi_{dp} & 0 \\ 0 & 0 & 1 \end{bmatrix} \begin{bmatrix} \cos\Psi_{pp} & -\sin\Psi_{pp} & 0 \\ \sin\Psi_{pp} & \cos\Psi_{pp} & 0 \\ 0 & 0 & 1 \end{bmatrix}$$
$$\cdot \begin{bmatrix} \cos\sigma_{pp} & 0 & \sin\sigma_{pp} \\ 0 & 1 & 0 \\ -\sin\sigma_{pp} & 0 & \cos\sigma_{pp} \end{bmatrix}$$
$$= \begin{bmatrix} \cos(\Psi_{pp}-\Psi_{dp}) & -\sin(\Psi_{pp}-\Psi_{dp}) & 0 \\ \sin(\Psi_{pp}-\Psi_{dp}) & \cos(\Psi_{pp}-\Psi_{dp}) & 0 \\ 0 & 0 & 1 \end{bmatrix}$$
$$\cdot \begin{bmatrix} \cos\sigma_{pp} & 0 & \sin\sigma_{pp} \\ 0 & 1 & 0 \\ -\sin\sigma_{pp} & 0 & \cos\sigma_{pp} \end{bmatrix}$$
$$= \boldsymbol{T}_{Z_v}^{\mathrm{T}}\left(\Psi_{pp}-\Psi_{dp}\right)\boldsymbol{T}_{Y_v}^{\mathrm{T}}\left(\sigma_{pp}\right). \tag{16}$$

The following equations can be obtained.

$$\Psi_{pp} = \Psi_{tr} + \Psi_{dp}$$
$$\sigma_{pp} = \sigma_{tr}$$

The following guidance laws can be obtained.

$$\Psi_d = \Psi_{tr} + \Psi_{pp} \tag{17}$$

$$\sigma_d = \sigma_{tr} \tag{18}$$

For the desired path of the powered parafoil in the phase of task execution, the coordinates of the desired point $\boldsymbol{p}_{dp}\left(\varpi\right)$ can be described as follows.

$$\begin{cases} x_{dp} = R\sin\left(\varpi\right) \\ y_{dp} = -R\cos\left(\varpi\right) \\ z_{dp} = H_d \end{cases}$$

where, R denotes the radius of the circular path, and H_d denotes the set flight altitude.

Proposition: In the phase of task execution, If the parameter ϖ of desired path is updated according to (19), and azimuth angle Ψ_{pp} and inclination angle σ_{pp} of the powered parafoil change with guidance laws (20), (21), respectively, the error set $\boldsymbol{\varepsilon}$ between the powered parafoil and the desired point $\boldsymbol{p}_{dp}$ is global uniformly asymptotically stable and local exponential stable.

$$\dot{\varpi} = \frac{U_{ve}\cos\Psi_{tr}\cos\sigma_{tr} + k_s s}{\sqrt{x_{dp}'^{\,2} + y_{dp}'^{\,2} + z_{dp}'^{\,2}}} \tag{19}$$

$$\Psi_d = \arctan\left(-\frac{e}{k_e}\right) + \arctan\left(\frac{y_{dp}'\left(\varpi\right)}{x_{dp}'\left(\varpi\right)}\right) \tag{20}$$

$$\sigma_d = \arctan\left(\frac{h}{k_h}\right) \tag{21}$$

Proof: Take the derivative of (11) with respect to the time.

$$\dot{\boldsymbol{\varepsilon}} = \dot{\boldsymbol{T}}_{I-p}\left(\boldsymbol{p}-\boldsymbol{p}_{dp}\right) + \boldsymbol{T}_{I-p}\left(\dot{\boldsymbol{p}}-\dot{\boldsymbol{p}}_{dp}\right) \tag{22}$$

where $\dot{\boldsymbol{T}}_{I-p} = \boldsymbol{S}\cdot\boldsymbol{T}_{I-p}$, and the matrix $\boldsymbol{S}$ can be expressed as follows.

$$\boldsymbol{S} = \begin{bmatrix} 0 & \dot{\Psi}_{dp}\cos\sigma_{dp} & -\dot{\sigma}_{dp} \\ -\dot{\Psi}_{dp}\cos\sigma_{dp} & 0 & -\dot{\Psi}_{dp}\sin\sigma_{dp} \\ \dot{\sigma}_{dp} & \dot{\Psi}_{dp}\sin\sigma_{dp} & 0 \end{bmatrix}$$

Deduce (22) further.

$$\dot{\boldsymbol{\varepsilon}} = \boldsymbol{S}\cdot\boldsymbol{T}_{I-p}\left(\boldsymbol{p}-\boldsymbol{p}_{dp}\right) + \boldsymbol{T}_{I-p}\left(\boldsymbol{T}_{I-p}^{\mathrm{T}}\boldsymbol{T}_{v-p}\boldsymbol{V}_{ve} - \boldsymbol{T}_{I-p}^{\mathrm{T}}\boldsymbol{V}_{dp}\right)$$
$$= \boldsymbol{S}\cdot\boldsymbol{\varepsilon} + \boldsymbol{T}_{v-p}\boldsymbol{V}_{ve} - \boldsymbol{V}_{dp} \tag{23}$$

Lyapunov function about error is defined.

$$V_\varepsilon = \frac{1}{2}\boldsymbol{\varepsilon}^{\mathrm{T}}\boldsymbol{\varepsilon} = \frac{1}{2}\left(s^2+e^2+h^2\right) \tag{24}$$

Take the derivative of (24) with respect to the time.

$$\dot{V}_\varepsilon = \boldsymbol{\varepsilon}^{\mathrm{T}}\dot{\boldsymbol{\varepsilon}}$$
$$= \boldsymbol{\varepsilon}^{\mathrm{T}}\left(\boldsymbol{S}\cdot\boldsymbol{\varepsilon} + \boldsymbol{T}_{v-p}\boldsymbol{V}_{ve} - \boldsymbol{V}_{dp}\right)$$
$$= \boldsymbol{\varepsilon}^{\mathrm{T}}\boldsymbol{S}\boldsymbol{\varepsilon} + \boldsymbol{\varepsilon}^{\mathrm{T}}\left(\boldsymbol{T}_{v-p}\boldsymbol{V}_{ve} - \boldsymbol{V}_{dp}\right) \tag{25}$$

After simplification,

$$\dot{V}_\varepsilon = s\left(U_{ve}\cos\Psi_{tr}\cos\sigma_{tr} - U_{dp}\right) + eU_{ve}\sin\Psi_{tr}\cos\sigma_{tr}$$
$$-hU_{ve}\sin\sigma_{tr} \tag{26}$$

Let U_{dp} satisfy the following equation.

$$U_{dp} = U_{ve}\cos\Psi_{tr}\cos\sigma_{tr} + k_s s \tag{27}$$

where, k_s is a positive parameter. On condition that the velocity of the desired point satisfies (27), the first term on the right of (26) is always less than or equal to zero.

Let Ψ_{tr}, σ_{tr} satisfy the following equations, respectively.

$$\Psi_{tr} = \arctan\left(-\frac{e}{k_e}\right) \tag{28}$$

$$\sigma_{tr} = \arctan\left(\frac{h}{k_h}\right) \tag{29}$$

where k_e, k_h are the adjustable positive parameters. Substituting (27), (28), (29) into (26), the following equation can be obtained.

$$\dot{V}_\varepsilon = -k_s s^2 - U_{ve}\left(\cos\sigma_{tr}\frac{e^2}{\sqrt{e^2+k_e^2}} + \frac{h^2}{\sqrt{h^2+k_h^2}}\right) \tag{30}$$

$\sigma_{tr} \in \left(-\frac{\pi}{2}, \frac{\pi}{2}\right)$, such that $\cos\sigma_{tr} \geq 0$, which guarantees $\dot{V}_\varepsilon < 0$.

Scaling variable ϖ of the desired path is updated by (19) to eliminate the forward error s. The control objective is to design control laws with guidance laws. Only lateral and vertical controllers are needed to make azimuth angle Ψ_{pp} track Ψ_d to eliminate lateral error *e*, and inclination angle σ_{pp} track σ_d to eliminate vertical error *h*, respectively.

4. DESIGN OF LADRC CONTROLLERS

Compared with the common parafoil system, the model of the powered parafoil is more complicated, and there exist modeling errors in the process of modeling. The motion in horizontal plane is controlled through pulling the steering line, and the vertical motion is controlled by the thrust provided by the engine propeller system. Because of the non-rigid connection between the canopy and payload, and the strong coupling between the horizontal motion and the vertical motion, it is very difficult for the precision control of the powered parafoil. And uncertainties of the model caused by flexibility increase difficulty of control. Based on the considerations above, linear active disturbance rejection control (LADRC) (Gao, 2003, 2006) is applied to the controller design, whose adjustable parameters are less, compared with ADRC.

4.1 Theory of LADRC

On the basis of control algorithm of ADRC, LADRC adopts linear ESO and feedback control law, which simplify the control parameters, such that LADRC is easier for the practical engineering application. For the traditional second-order controlled object, shown as (31)

$$\ddot{y}_o = f\left(\dot{y}_o, y_o, \Delta\right) + bu_{in}, \tag{31}$$

where y_o is output, and u_{in} is input. Δ is disturbance. b is the system parameter. f is the function about $\dot{y}_o$, y_o, Δ, which can be observed through linear ESO, shown as follows.

$$\begin{cases} \dot{\boldsymbol{z}} = \boldsymbol{Az} + \boldsymbol{B}u_{in} + \boldsymbol{L}\left(y_o - \hat{y}_o\right) \\ \hat{y}_o = \boldsymbol{Cz} \end{cases} \tag{32}$$

where $\boldsymbol{A} = \begin{bmatrix} 0 & 1 & 0 \\ 0 & 0 & 1 \\ 0 & 0 & 0 \end{bmatrix}$, $\boldsymbol{B} = \begin{bmatrix} 0 \\ b \\ 0 \end{bmatrix}$, $\boldsymbol{C} = \begin{bmatrix} 1 & 0 & 0 \end{bmatrix}$. $\boldsymbol{z}$ is observed value of states. $\boldsymbol{L}$ is the gain vector of the linear ESO, and $\boldsymbol{L} = [3\omega_o, 3\omega_o^2, \omega_o^3]^{\mathrm{T}}$, where ω_o is called as band width of linear ESO.

The linear ESO can observe the total disturbance of the system *f*, and compensate the observation value z_3 of *f*.

Letting

$$u_{in} = u_0 - \frac{z_3}{b}, \tag{33}$$

the expression of the second-order system can be transformed as follows.

$$\begin{aligned} \ddot{y}_o &= f\left(\dot{y}_o, y_o, \Delta\right) + bu_{in} \\ &= f\left(\dot{y}_o, y_o, \Delta\right) - z_3 + bu_0 \\ &\approx bu_0 \end{aligned} \tag{34}$$

The feedback control law u_0 adopts the form of linear PD, shown as (35).

$$u_0 = k_p(y_d - z_1) + k_d\left(\dot{y}_d - z_2\right) \tag{35}$$

Equations (32), (33), (35) constitute the LADRC of the second-order system, whose structural diagram is shown as Fig. 2.

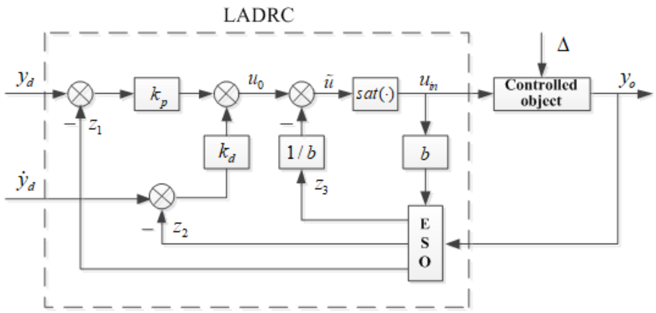

Fig. 2. LADRC structural diagram for the second order system.

In Fig. 2, LADRC is mainly composed of linear ESO and feedback control law, whose core is ESO. y_d represents the set value, and z_1, z_2, z_3 represent the observed values of states. $sat(\cdot)$ is the saturation function which prevents instability of system resulting from overcontrolling.

4.2 Design of LADRC Controllers in Two Channels

According to guidance commands, design of controller is divided into lateral and vertical channels. In lateral channel, the control objective is to eliminate lateral error form the desired point on the desired path. The azimuth angle of the powered parafoil is shown as follows.

$$\Psi_{pp}(t) = \arctan\left(\frac{\dot{y}}{\dot{x}}\right),$$

where, *x*, *y* denote the positon information of the powered parafoil in horizontal plane.

According to the dynamic model of the powered parafoil, the second order equation of the azimuth angle is obtained as follows, which is not a precise model.

$$\ddot{\Psi}_{pp}(t) = f_1(\cdot) + f_2\left(u_{in}\right) \tag{36}$$

$f_1(\cdot)$ denotes the function of system states. $f_2\left(u_{in}\right)$ denotes the function of control variable, from which the control variable cannot be separated. u_{in} represents the control variable. For azimuth angle control, the control variable is the deflection of trailing edge of the canopy δ. To facilitate design of LADRC controller, (36) can be transformed into the following equation.

$$\ddot{\Psi}_{pp}(t) = f_1(\cdot) + f_2\left(u_{in}\right) - b_0 u_{in} + b_0 u_{in} \tag{37}$$

b_0 is an adjustable parameter. Let $f = f_1(\cdot) + f_2\left(u\right) - b_0 u_{in}$. Regard *f* as the total disturbance in lateral plane, which need not be considered when designing controller. According to (32), ESO about the azimuth angle is constructed to observe and eliminate the disturbance. The control law is chosen as (33).

In vertical channel, the output state is the inclination angle σ_{pp}, and the control variable is the forward thrust that provided by the engine propeller. Applying the same principle, the vertical LADRC controller is designed. The overall control block diagram of the powered parafoil is shown as follows.

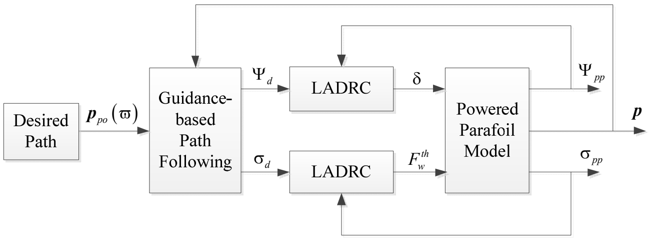

Fig. 3. The overall control block diagram.

5. SIMULATION ANALYSIS

The control method of the powered parafoil in the phase of task execution is discussed in this paper, where the path in horizontal plane is circular and the altitude is unchanged.

Disturbance in lateral and vertical channels is added in simulation experiment respectively to verify the performance of decoupling and disturbance rejection. Simulation parameters are given as follows.

The set radius of the circular path R=250m, and the altitude $H_d = 1970m$. The initial position of the powered parafoil is (0 -300 2000)m. The parameters of the powered parafoil model are referred to (Zhu et al., 2015). The control parameters are as follows.

The parameters of guidance law: $k_s = 0.5$, $k_e = 40$, $k_h = 60$.

The parameters of lateral LADRC controller: ω_o=30, k_p=3, k_d=18, b_0=0.2.

The parameters of vertical LADRC controller: ω_o=30, k_p=230, k_d=150, b_0=0.01.

The simulation time is 200s. To verify the anti-interference performance of the controller, the classical gust model of NASA is added to the simulation at 100s. Figs. 4-8 show the following performance of the powered parafoil when adding 3m/s gust along Y axis of ERF in horizontal plane.

Figs. 4-5 show the spatial path following control performance. The powered parafoil can follow the desired path, and path following curves are smooth and stable. Fig.6 shows path following control errors curves. The forward error s, lateral error e converge to zero at about 33s, and vertical error h converges to zero at about 25s. Under the influence of 3m/s gust along Y axis, the maximum lateral error is 0.2m, and the maximum vertical error is 0.5m.

Figs. 7-8 show control outputs of lateral and vertical channels. When the system converges, deflection percentage of trailing edge of the canopy is 7%, and thrust is 250N. There exists coupling between lateral and vertical channels, such that when the gust disturbance is added in lateral channel, the control variable in vertical channel is influenced, which results in the deviation of altitude, illustrated as Fig. 8. Through observing of ESO and compensating of controller, the internal coupling and external disturbance can be eliminated.

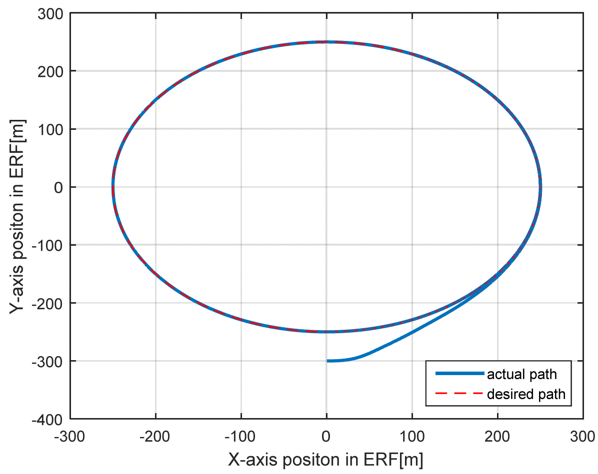

Fig. 4. Horizontal position control curves.

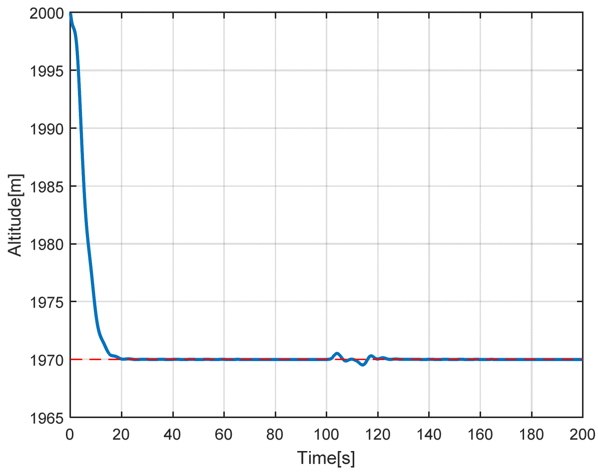

Fig. 5. Altitude control curves.

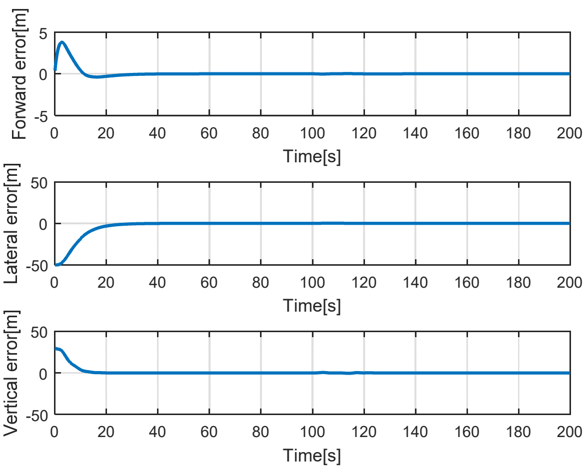

Fig. 6. Path following control errors curves.

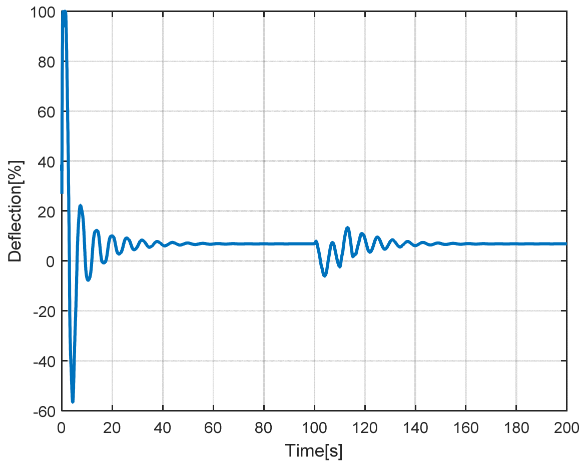

Fig. 7. Deflection percentage of trailing edge of the canopy.

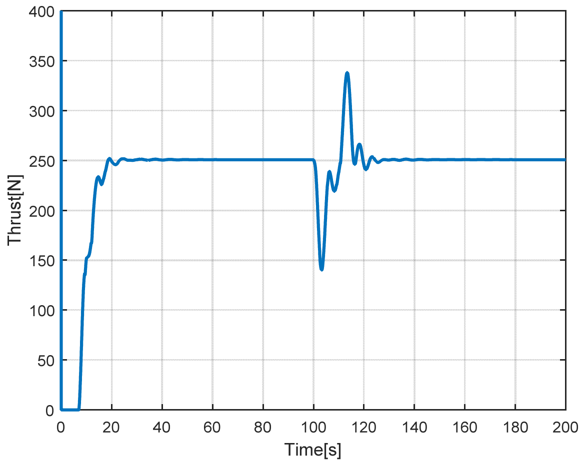

Fig. 8. Thrust curve.

Figs. 9-13 show the control performance of the powered parafoil when adding 3*m/s* gust along Z axis of ERF.

According to Figs. 9-11, before the 3*m/s* gust along Z axis of ERF is added, the control performances are the same as above simulation. After adding the gust along Z axis, the maximum vertical error is 1.3*m*, and the maximum lateral error is 0.1*m*.

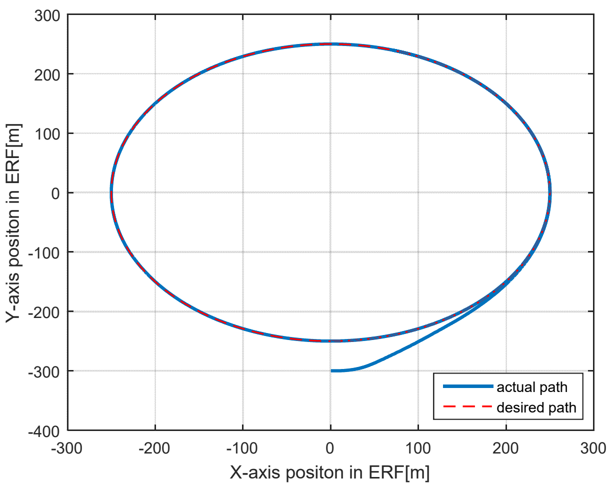

Fig. 9. Horizontal position control curves.

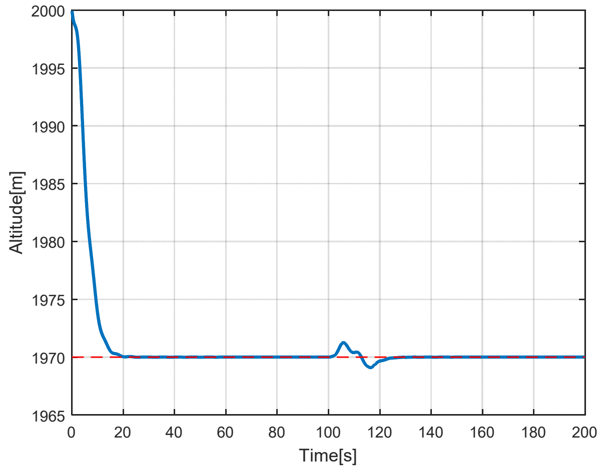

Fig. 10. Altitude control curves.

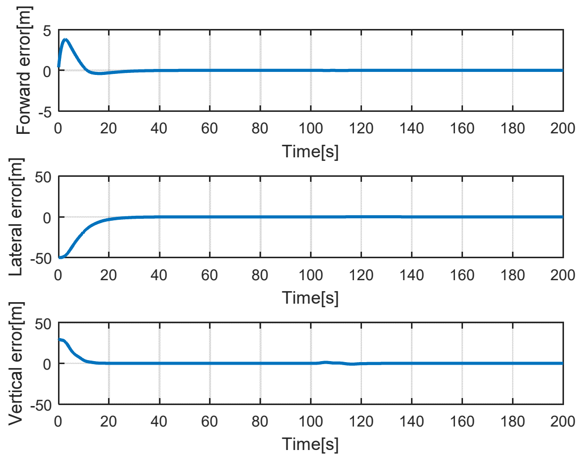

Fig. 11. Path following control errors curves.

Figs. 12-13 show control outputs of lateral and vertical channels. Similarly, the disturbance in vertical plane also influences the motion states of the powered parafoil in horizontal plane. Affected by gust, the altitude deviates from the set value, and the thrust decreases correspondingly, shown as Fig. 13. With adjusting of LADRC, control outputs achieve convergence again. Deflection percentage of trailing edge of the canopy is still 7%, and thrust is still 250*N*.

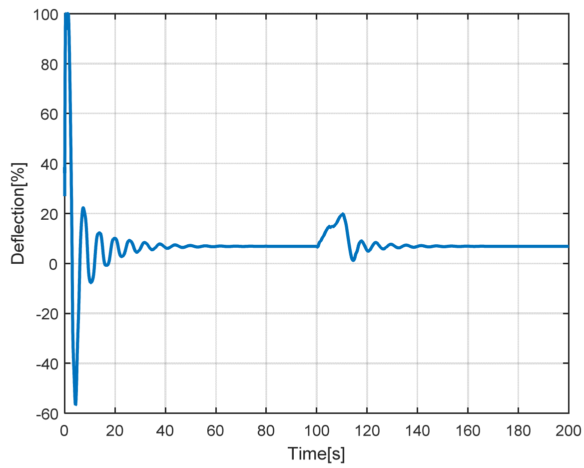

Fig. 12. Deflection percentage of trailing edge of the canopy.

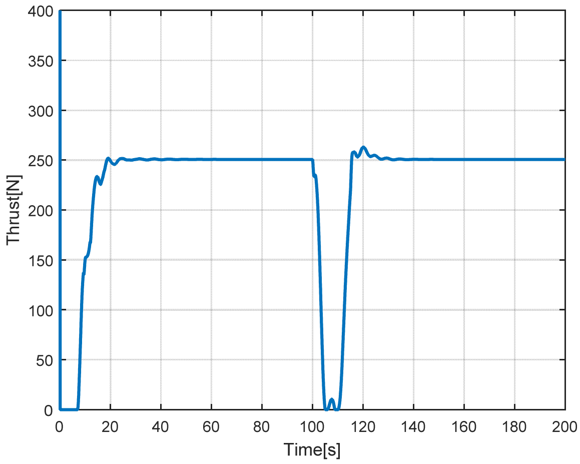

Fig. 13. Thrust curve.

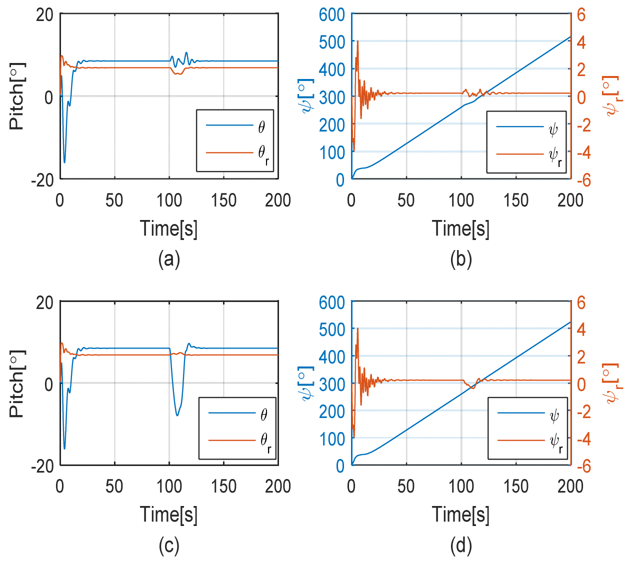

Fig. 14. Curves of angles of pitch and yaw.

Fig. 14 indicates changes of pitch angles and yaw angles. (a) and (b) show changing curves of pitch angles and yaw angles adding 3*m/s* gust along Y axis, respectively. (c) and (d) show changing curves adding 3*m/s* gust along Z axis. The powered parafoil follows the circular path, such that the yaw angle increases linearly. The relative yaw angle between the parafoil and the payload is about 0.2° because of the small deflection of trailing edge of the canopy. The pitch angle and relative pitch angle stabilized at about 8.5° and 6.9° , respectively. Under the influence of gust, attitudes angles fluctuate accordingly, but eventually stabilize. According to the motion characteristics of the powered parafoil, the pitch angle increases with increase of the thrust, which results in the increase of the angle of attack. Excessive angle of attack may cause the powered parafoil instability. In the process of control law design, in addition to the accurate path following, attitude angles must be stable and the control outputs need to be limited appropriately.

It is indicated that the guidance-based path following is stable, and the path is smooth. Adding gust disturbance to lateral and vertical channels respectively, controllers can observe and compensate effectively. LADRC still shows good anti-disturbance performance.

6. CONCLUSIONS

Aiming at the non-rigid flexible vehicle, a guidance-based path following control method for the powered parafoil was presented. The desired path was parameterized by scaling variable. Through Lyapunov method, the position error from the desired path was transformed to guidance commands of azimuth angle and inclination angle for lateral channel and vertical channel. Two LADRC controllers were designed for guidance commands control. As for system coupling and gust disturbance, ESO was constructed in each channel to observe the total disturbance. The path following strategy is stable and smooth, and the control method is easy to implement in engineering. Simulation results verified its validity.

The guidance-based path following is only suit for the regular shape path, and the altitude of the desired path in this paper is unchanged. The future work will focus on the spatial irregular shape path following control. In addition, the parameter tuning method of LADRC based on stability margin also should be studied.

ACKNOWLEDGMENT

This work was supported by the Project of Program for Excellent Young Talents in Universities of Anhui Province under Grant No. gxyq2017045 and Anhui Natural Science Foundation under Grant No. 1808085MF183.

REFERENCES

Aoustin, Y. and Martinenko, Y. (2012). Control algorithms of the longitude motion of the powered paraglider. *Proceedings of the Biennial Conference on Engineering Systems Design and Analysis*, Nantes, France, pp. 775-784.

Barrows, T. (2002). Apparent mass of parafoil with spanwise camber. *Journal of Aircraft*, vol. 39, no. 3, pp. 445-451.

Breivik, M. and Fossen, T. (2005). Principles of guidance-based path following in 2D and 3D. *Proceedings of the 44th IEEE Conference on Decision and Control, and the European Control Conference*, Seville, Spain, pp. 627-634.

Breivik, M. and Fossen, T. (2008). Guidance laws for planar motion control. *Proceedings of the 47th IEEE Conference on Decision and Control*, Cancun, Mexico, pp. 570-577.

Chambers, J. (2007). Longitudinal dynamic modeling and control of powered parachute aircraft. *Ph.D. thesis,* Rochester Institute of Technology.

Chen, Z. L. and Zhang, H. (2016). Altitude control for unmanned powered parafoil based on backstepping method, *2016 Chinese Control and Decision Conference*, Yinchuan, pp. 5058-5064.

Chen, S. Sun, Q. L. Luo S. Z. et al. (2017). Longitudinal Control of Unmanned Powered Parafoil with Precise Control Gain, *Proceedings of 2017 Chinese Intelligent Systems Conference*, Singapore, pp. 89-98.

Goodrick, T. (1981). Comparison of simulation and experimental data for a gliding parachute in dynamic flight. *AIAA* 1981-1924

Gao, Z.Q. (2003). Scaling and bandwidth-parameterization based controller tuning. *Proceedings of the 2003 American Control Conference*, Denver, CO, United States, pp. 4989-4996.

Gao, Z.Q. (2006). Active disturbance rejection control: a paradigm shift in feedback control system design. *Proceedings of the 2006 American Control Conference*, Minneapolis, MN, United States, pp. 2399-2405.

Ghoreyshi, M. Bergeron, K. Jirasek, A. et al. (2016). Computational aerodynamic modelling for flight dynamics simulation of ram-air parachutes. *Aerospace Science and Technology*, no. 54, pp. 286-301.

Li, B. B. Qi, J. T. et al. (2015). Real-Time Data Acquisition and Model Identification for Powered Parafoil UAV, *International Conference on Intelligent Robotics & Applications*. Springer International Publishing, pp. 556-567.

Muller, S. Wagner, O. Sachs, G. (2003). A high-fidelity nonlinear multibody simulation model for parafoil systems. *17th AIAA Aerodynamic Deceleretor Systems Technology Conference and Seminar*, Monterey, CA, United States, pp. 2003-2120.

Ochi, Y. Kondo, H. Watanabe, M. (2009). Linear dynamics and PID flight control of a powered paraglider. *AIAA Guidance, Navigation and Control Conference and Exhibit*, Chicago, IL, United States, pp. 2009-6318.

Slegers, N. Yakimenko, O. (2009). Optimal control for terminal guidance of autonomous parafoils. AIAA 2009-2958.

Slegers, N. (2010). Effects of canopy-payload relative motion on control of autonomous parafloils, *Journal of Guidance, Control, and Dynamics*, vol. 33, no.1, pp. 116-125.

Tao, J. Sun, Q. L. Chen, Z. Q. et al. (2016). Modeling and Simulation of Parafoil Systems in Wind Fields, *Proceedings of 2016 Chinese Intelligent Systems Conference*, Singapore, pp. 109-117.

Tan, P. L. Sun, Q. L. Jiang, Y. X. et al. (2017). Trajectory tracking of powered parafoil based on characteristic model based all-coefficient adaptive control, *Journal of Central South University*, vol. 24, no.24, pp. 1073-1081.

Watanabe, M. and Ochi, Y. (2008). Modeling and simulation of nonlinear dynamics of a powered paraglider, AIAA 2008-7418.

Xiong, J. (2005). Research on the dynamics and homing project of parafoil system, *Ph.D. thesis*, National University of Defense Technology.

Xiang, X. Lapierre, L. et al. (2009). Coordinated path following control of multiple nonholonomic vehicles, *Oceans IEEE*, pp. 1-7.

Yang, H. Song, L. et al. (2013). Study on powered-parafoil longitudinal flight performance with a fast estimation model, *Journal of Aircraft*, vol. 50, no. 5, pp. 1660-1667.

Zheng, Z. W. Huo, W. (2013a). Planar path following control for stratospheric airship, *IET Control Theory and Applications*, vol. 7, no. 2, pp. 185-201.

Zheng, Z. W. Wu, Z. (2013b). Global path following control for underacuated stratospheric airship, *Advances in Space Research*, vol. 52, no. 7, pp. 1384-1395.

Zheng, Z. W. Huo, W. et al. (2014). Direct-adaptive fuzzy path following control for an autonomous airship, *Control and Decision*, vol. 29, no. 3, pp. 418-424.

Zhu, E. L. Sun, Q. L. et al. (2015). Modeling of powered parafoil based on kirchhoff motion equation, *Nonlinear Dynamics*, vol. 79, no. 1, pp. 617-629.

Zhang, Z. X. Zhao, Z. N. Fu, Y. L. (2018). Dynamics analysis and simulation of six DOF parafoil system, *Cluster Computing*, no. 2, pp. 1-12.